Journal of Organometallic Chemistry 880 (2019) 300–311

Contents lists available at ScienceDirect

Journal of Organometallic Chemistry

journal homepage: www.elsevier.com/locate/jorganchem

Impact of bidentate *N*,C-Chelate ligands on the performance of phosphorescent Pt(II) complexes as oxygen sensors

Faraz Hussain, Xiang Wang, Suning Wang*

Department of Chemistry, Queen's University, Kingston, Ontario, K7L 3N6, Canada

ARTICLE INFO

Article history:
Received 23 October 2018
Received in revised form
9 November 2018
Accepted 12 November 2018
Available online 19 November 2018

This article is dedicated to Professor Richard Puddephatt in celebration of his 75th birthday

Keywords:
Pt(II) complexes
N,C-chelate ligands
Phosphorescence
Oxygen sensors

ABSTRACT

A library of 1,2- cyclometalated Pt(II) complexes based on various bidentate *N*,C-chelate chromophores have been studied for their uses as luminescent oxygen sensing probes (OSPs). The bidentate chelate ligands have been found to have a distinct impact on the performance of the Pt(II) compounds as OSPs. For some of the complexes, attachment of a dimesityl boron group ($BMes_2$) to the chelate ligands enhances their oxygen sensitivity. For phenyl-1,2,3-triazole (Phtrz) based Pt(II) complexes, the attachment of a diphenyl amino moiety to the *N*,C-chelate ligand substantially enhances phosphorescence quenching and the performance of the OSP. A high K_{SV}^{app} value (0.0667 $Torr^{-1}$) for the OSP based on the diphenyl amino functionalized Pt(II) complex was achieved, which is the highest value reported to date for OSPs based on bidentate Pt(II) complexes.

1. Introduction

The detection of molecular oxygen is of great importance in the fields of medicine and biology [1]. Of the known oxygen sensing methods, optical sensing has attracted much attention owing to reusability, low fabrication cost and quick response times of the sensory devices. Luminescent oxygen sensing probes (OSPs) are based on dynamic quenching by oxygen, that leads to a change of luminescence intensity and decay lifetimes. Transition metal complexes are commonly used as OSPs because their long-lived phosphorescence leads to increased sensitivity towards oxygen. Many examples of OSPs based on Ir(III) [2], Ru(II) [3], Os(II) [4] and Ln(III) [5] complexes have been demonstrated in the literature. However, Pt(II) based OPSs remain relatively rare. Therefore, the motivation of this study is to expand the scope of Pt(II) based OPSs by examining the performance of a variety of Pt(II) complexes with bidentate *N*,C-chelate and ancillary ligands developed by our group. In particular, several new dimesitylboron functionalized Pt(II) complexes were obtained and examined for OPS performance. The triarylboron functionalization strategy was demonstrated previously to be highly effective in achieving bright phosphorescent compounds [6–8], enabling their applications as efficient emitters for OLEDs or sensors for anions. Triarylboron-functionalized metal complexes have however not been studied for OSPs applications. A comparative study with highly emissive, non-boron functionalized analogues developed recently by our lab was also performed to establish the influence of the various functional groups on the performance of the Pt(II) based OPSs. Four representative classes of Pt(II) compounds are investigated in this study, which include the pyridyl-indole chelate compounds **1** [9], **2**, **3**, the benzofuran-pyridyl chelate compounds **4** [9] and **5** [6], the benzothiophene-pyridyl compounds **6** [9], **7** [6], and the phenyl-triazole chelate compounds **8**–**10** [7] and **11**–**12** [8] shown in Fig. 1. Our investigation established that the chelate ligands have a distinct impact on the performance and the photostability of the Pt(II) complexes in OPSs. The details are presented herein.

2. Experimental

All reactions were carried out under a nitrogen atmosphere unless otherwise noted. Reagents were purchased from commercial suppliers and used as received. TLC and flash chromatography were performed on silica gel. Samples for ^{1}H and ^{13}C NMR were prepared using solvents purchased from Cambridge Isotope Laboratories, Inc.

* Corresponding author.
E-mail address: sw17@queensu.ca (S. Wang).

https://doi.org/10.1016/j.jorganchem.2018.11.017
0022-328X/

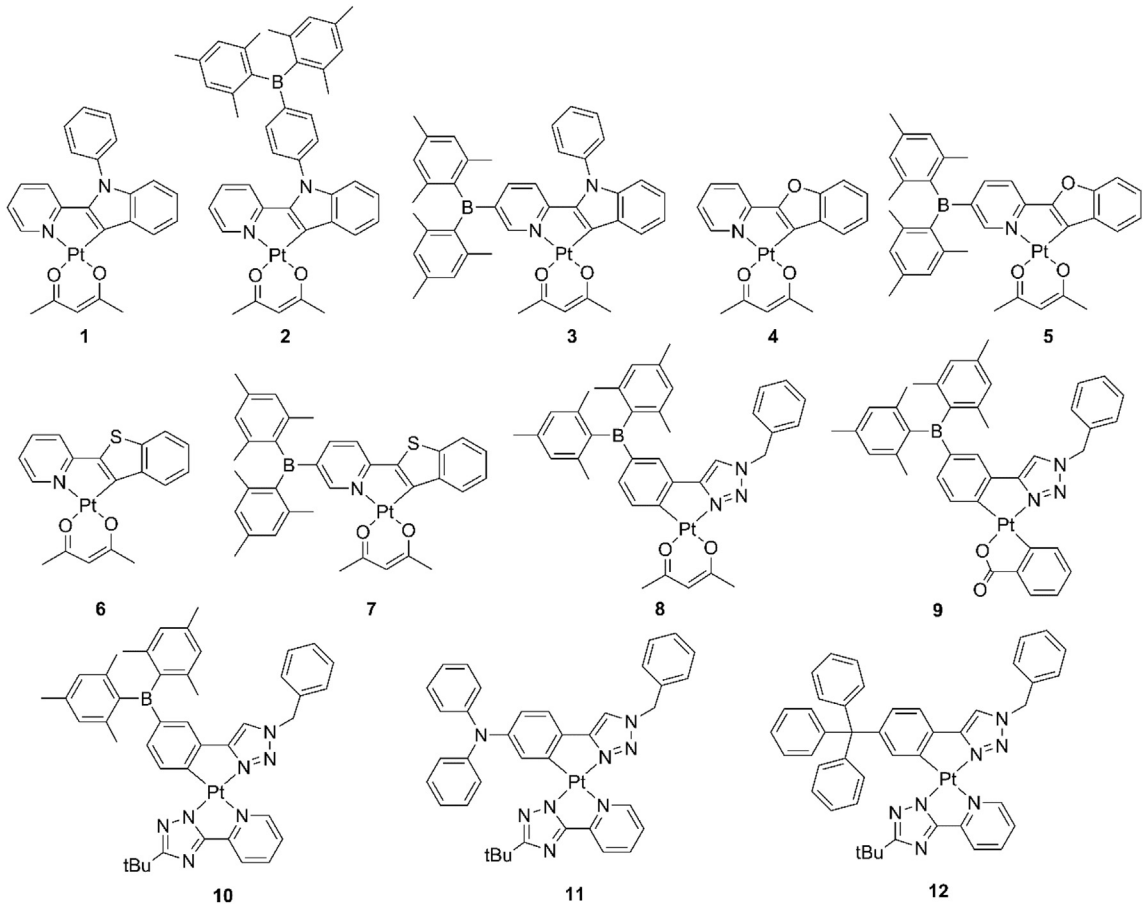

Fig. 1. Molecular structures of Pt(II) compounds examined for OPS applications in this work.

and were recorded on a Bruker Avance 400, 500 or 700 MHz spectrometer. Elemental analysis was performed by the Analytical and Instrumentation Laboratory at the University of Alberta. Emission spectra were obtained on a Photon Technologies International QuantaMaster Model 2 spectrometer. Solution quantum yields were determined using a Hamamatsu C11347-11 Quantaurus-QY spectrometer. UV–Visible spectra were recorded using a Varian Carry 50 UV/Vis spectrophotometer. The crystal structural data of **2** was collected on a Bruker D8 Venture X-ray single crystal diffractometer with Mo Kα radiation at 180 K. Data were processed using the Bruker APEX III software and SHELXTL software package (SHELXTL-2014/7). The crystal data of **2** was deposited at the Cambridge Crystallographic Data Center (CCDC No. 1873920). TD-DFT calculations were carried out using the Gaussian 09 software [10] at the High Performance Computing Virtual Laboratory (HPCVL) at Queen's University. All computations were performed at the B3LYP level of theory using LANL2DZ as the basis set for Pt and 6-31G(d) for all other atoms. Compounds **1** and **4**–**12** were previously reported with full characterization data.

2.1. Syntheses of ligands

1-(4-bromophenyl)-2-(pyridin-2-yl)-1H-indole [11] and 1-phenyl-1H-indole [12] were prepared following the procedure reported in the literature.

1-(4-(dimesitylboryl)phenyl)-2-(pyridin-2-yl)-1H-indole (**L1**, 72% yield): 1-(4-bromophenyl)-2-(pyridin-2-yl)-1H-indole (0.40 g, 1.15 mmol) was added to an oven dried Schlenk flask under N_2. After the addition of dry THF (30 mL), the reaction mixture was cooled to −100 °C and n-BuLi (0.50 mL, 1.30 mmol, 2.5 M, hexane) was added dropwise. After 40 min of stirring at −100 °C, $FBMes_2$ (0.34 g, 1.3 mmol) was added to the flask and the reaction mixture was slowly warmed to room temperature and stirred overnight. The mixture was extracted with CH_2Cl_2 and purified by flash chromatography (4:1 hexane/ethyl acetate) yielding a white solid. ^{1}H NMR (400 MHz, $CDCl_3$): δ 8.50 (dt, $J = 4.6$, 1.5 Hz, 1H, py-H), 7.77–7.72 (m, 1H, indole-H), 7.61–7.55 (m, 2H, ph-H), 7.50 (td, $J = 7.8$, 1.8 Hz, 1H, py-H), 7.42–7.35 (m, 1H, indole-H), 7.28–7.20 (m, 4H, ph-H, indole-H), 7.19–7.10 (m, 3H, py-H, indole-H), 6.86 (s, 4H, Mes-H), 2.33 (s, 6H, Mes-H), 2.07 (s, 12H, Mes-H). ^{13}C NMR (176 MHz, $CDCl_3$): δ 151.25, 149.40, 144.90, 142.00, 141.61, 140.81, 139.43, 139.21, 138.92, 137.14, 135.61, 128.31, 128.21, 127.28, 123.35, 123.31, 121.73, 121.37, 121.03, 110.79, 106.34, 23.45, 21.26. HRMS (ESI) calculated for $C_{37}H_{35}BN_2$ $[M+H]^+$: calcd 518.2893; found, 518.2900.

2-(5-bromopyridin-2-yl)-1-phenyl-1H-indole (**BI1**, 54% yield): 1-phenyl-1H-indole (2.0 g) was added to an oven dried Schleck flask under N_2. With a syringe, 2,2,6,6-tetramethylpiperidine (3.27 g, 23 mmol) and N,N,N′,N′-tetramethylethylenediamine (5.93 g, 51 mmol) were added to the reaction flask followed by the addition of dry hexane (40 mL). The mixture was cooled to 0 °C before n-BuLi (9.27 mL, 23 mmol, 2.5 M) was added dropwise. After 5 min, $ZnCl_2$-TMEDA (1.95 g, 8 mmol) was slowly added to the reaction flask. After stirring the reaction mixture for 2 h at 0 °C, the solvent was removed under an inert atmosphere. The residue was dissolved in dry THF (40 mL) before $Pd(PPh_3)_4$ (0.798 g, 0.70 mmol) and 2-iodo-5-bromopyridine (2.24 g, 11 mmol) were added. The reaction mixture was refluxed at 55 °C overnight, extracted with

CH_2Cl_2 and purified by column chromatography (100:1 hexane/ethyl acetate) to afford a white solid. ^{1}H NMR (500 Hz, CD_2Cl_2): δ 8.60 (d, J = 2.4 Hz, 1H, py-H), 7.75 (dd, J = 7.2, 1.6 Hz, 1H, indole-H), 7.64 (dd, J = 8.5, 2.4 Hz, 1H, py-H), 7.49 (dd, J = 8.4, 6.8 Hz, 2H, ph-H), 7.43 (m, 1H, indole-H), 7.35–7.29 (m, 2H, indole-H), 7.27–7.18 (m, 2H, indole-H), 7.03 (d, J = 8.4 Hz, 1H, py-H). ^{13}C NMR (126 MHz, $CDCl_3$): δ 150.59, 149.69, 139.91, 138.74, 138.44, 138.38, 129.43, 127.91, 127.87, 127.53, 124.00, 123.53, 121.35, 121.05, 118.73, 110.92, 106.44. HRMS (ESI) calculated for $C_{19}H_{13}BrN_2$ $[M+H]^+$: calcd., 348.0262; found, 348.0269.

2-(5-(dimesitylboryl)pyridin-2-yl)-1-phenyl-1H-indole (**L2**, 64% yield): An oven dried Schlenk flask under N_2 was charged with 2-(5-bromopyridin-2-yl)-1-phenyl-1H-indole (0.40 g, 1.2 mmol). After the addition of dry THF (50 mL) the flask was cooled to −100 °C and n-BuLi (0.50 mL, 1.3 mmol, 2.5 M) was added dropwise. After stirring for 40 min, $FBMes_2$ (0.36 g, 1.3 mmol) was added to the reaction flask. The reaction mixture was slowly warmed to room temperature over 12 h and extracted with CH_2Cl_2. **L2** was purified by column chromatography (150:1 hexane/ethyl acetate) to obtain a yellow solid. ^{1}H NMR (400 Hz, CD_2Cl_2): δ 8.59 (s, 1H, py-H), 7.75 (m, 1H, indole-H), 7.59 (dd, J = 7.9, 1.9 Hz, 1H, py-H), 7.51–7.39 (m, 3H, ph-H and indole-H), 7.35–7.27 (m, 4H, ph-H and indole-H), 7.26–7.16 (m, 3H, Py-H and indole-H), 6.87 (s, 4H, Mes-H), 2.33 (s, 6H, Mes-H), 2.03 (s, 12H, Mes-H). ^{13}C NMR (126 MHz, $CDCl_3$): δ 156.89, 153.39, 143.54, 140.71, 140.23, 139.34, 139.15, 139.04, 130.93, 129.58, 129.26, 129.10, 128.86, 128.37, 128.00, 127.91, 127.45, 123.62, 122.21, 121.48, 120.97, 110.90, 107.24, 23.53, 21.24. HRMS (ESI) calculated for $C_{37}H_{35}BN_2$ $[M+H]^+$: calcd., 518.2893; found, 518.2906.

2.2. Syntheses of Pt(II) complexes

Compounds **1**, **4**–**12** were prepared according to previously reported procedures [6–9].

Compounds **2** and **3** were prepared following a one-pot procedure [9].

2 (82% yield): **L1** (0.35 mmol) and $[PtMe_2(SMe_2)]_2$ (0.17 mmol) were dissolved in 30 mL of dry THF. The reaction was stirred for 1 h and followed by the dropwise addition of *p*-tolunesulfonic acid solution (1 mL, 0.35 M in THF) at ambient temperature. After 30 min of stirring, a solution of sodium acetylacetonate (0.70 mmol in 2 mL MeOH) was added. After stirring for 1.5 h, the mixture was extracted with CH_2Cl_2 and purified by column chromatography. ^{1}H NMR (400 Hz, CD_2Cl_2): δ 8.95 (ddd, J = 5.8, 1.6, 0.8 Hz, 1H, py-H), 8.25 (ddd, J = 7.9, 1.3, 0.8 Hz, 1H, indole-H), 7.75–7.63 (m, 2H, ph-H), 7.51–7.38 (m, 3H, ph-H and py-H), 7.24 (ddd, J = 8.2, 6.8, 1.3 Hz, 1H, indole-H), 7.18–7.09 (m, 2H, two indole-H), 6.94–6.85 (m, 5H, Mes-H and py-H), 6.52 (ddd, J = 8.2, 1.4, 0.8 Hz, 1H, py-H), 5.61 (s, 1H, acac-H), 2.35 (s, 6H, Mes-H), 2.12 (s, 12H, Mes-H), 2.10 (s, 3H, acac-H), 2.06 (s, 3H, Mes-H). ^{13}C NMR (176 MHz, $CDCl_3$): δ 184.95, 183.54, 159.63, 148.20, 142.30, 141.97, 141.57, 140.77, 139.02, 137.88, 137.50, 132.98, 128.37, 127.44, 124.39, 123.72, 120.53, 118.23, 117.70, 117.32, 110.01, 102.46, 28.27, 26.41, 23.49, 21.26. HRMS (ESI) calculated for $C_{42}H_{41}BN_2O_2Pt$ $[M+H]^+$: calcd., 811.2909; found, 811.2922.

3 (75% yield): Prepared using the same procedure as **3** except replacing **L1** with **L2**. ^{1}H NMR (400 Hz, $CDCl_3$): δ 8.99 (m, J = 1.5 Hz, 1H, py-H), 8.30 (d, J = 7.9 Hz, 1H, indole-H), 7.55 (dd, J = 8.2, 6.7 Hz, 2H, ph-H), 7.50–7.38 (m, 4H, py-H and ph-H), 7.22 (ddd, J = 8.2, 6.9, 1.3 Hz, 1H, indole-H), 7.11 (t, J = 7.4 Hz, 1H, indole-H), 7.01 (d, J = 8.2 Hz, 1H, indole-H), 6,84 (s, 4H, Mes-H), 6.31 (d, J = 8.3 Hz. 1H, py-H), 5.48 (s, 1H, acac-H), 2.30 (s, 6H, Mes-H), 2.09 (s, 12H, Mes-H), 2.07 (s, 3H, acac-H), 1.68 (s, 3H, acac-H). ^{13}C NMR (176 MHz, $CDCl_3$): δ 185.12, 183.35, 161.33, 157.20, 146.69, 143.26, 142.90, 140.65, 140.30, 138.82, 138.40, 132.85, 129.59, 128.32, 128.06, 125.29, 124.17, 122.03, 120.34, 116.01, 110.12, 102.24, 27.45, 26.45, 25.29, 21.16. HRMS (ESI) calculated for $C_{42}H_{41}BN_2O_2Pt$ $[M+H]^+$: calcd., 811.2909; found, 811.2922.

2.3. Oxygen sensing apparatus

Sensors as 5 wt% doped EC (ehtyl cellulose) films were prepared by dissolving EC (9.5 mg) and the Pt(II) compound (0.50 mg) in 1 mL of CH_2Cl_2. Thereafter, 0.50 mL of the solution was transferred to a quartz cuvette and was left to dry overnight to obtain the oxygen sensing film. The cuvette was then sealed with a rubber septum and used as a flow cell. Films at 1 wt% were prepared in the same way. The setup of the sensing apparatus is shown in Fig. 2.

2.4. Stern-Volmer fitting

To model the phosphorescent intensity changes of the EC films versus O_2 concentration, Stern-Volmer (SV) plots were constructed and fitted using the Demas two-site model (equation (1)) [13]. The equation takes the heterogenous quality of the films into account by allotting two quenching (k_{SV1} and k_{SV2}) and fractional

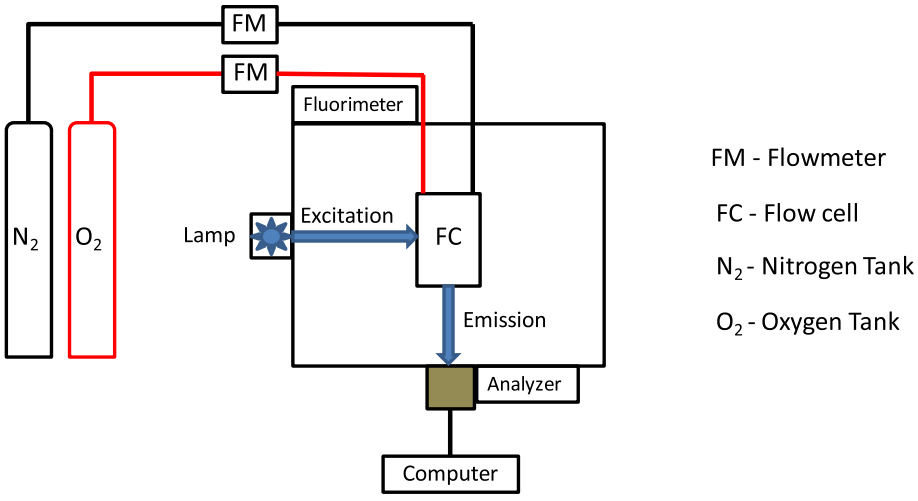

Fig. 2. The schematic presentation of the flow system designed and used for the evaluation of solid-state phosphorescence quenching of the OSPs doped in an EC polymer.

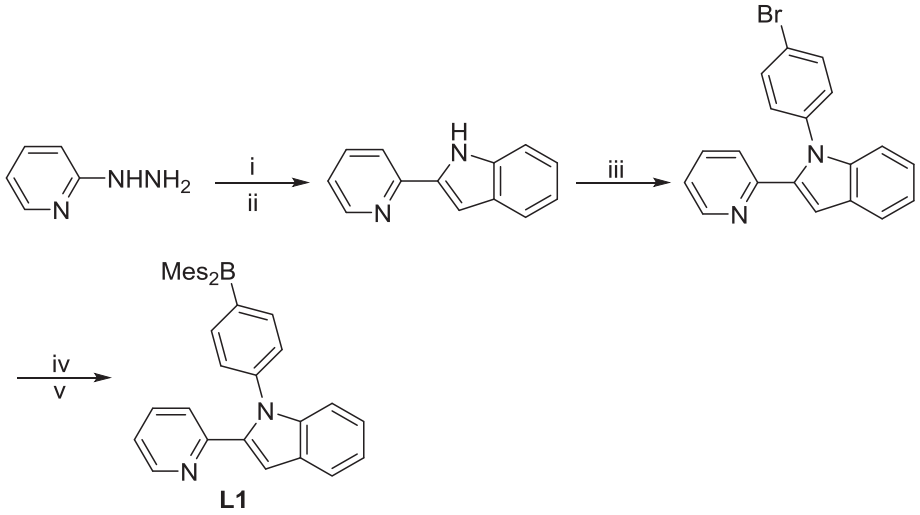

Scheme 1. Synthetic pathway for **L1**. Reaction conditions: (i) 2-acetylpyridine phenylhydrazone, polyphosphoric acid, reflux, 1.5 h; (ii) NaOH; (iii) 4-bromoiodobenzene, CuI, K_3PO_4, (±)-trans-1,2-diaminocyclohexane, 1,4-dioxane, reflux, 18 h; (iv) *n*-BuLi, THF, −100 °C; (v) $FBMes_2$, RT, 12 h.

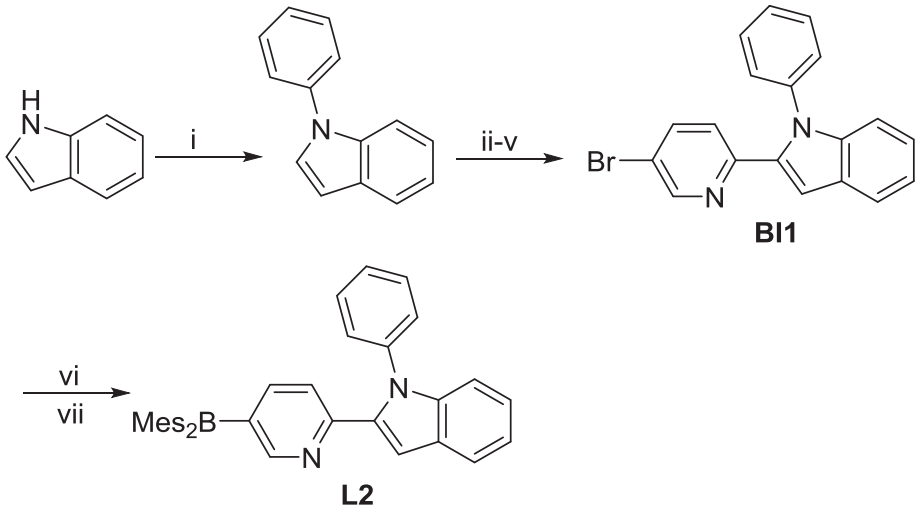

Scheme 2. Synthetic pathway for **BI1** and **L2**. Reaction Conditions: a) (i) iodobenzene, CuI, K_3PO_4, (±)-trans-1,2-diaminocyclohexane; (ii) TMEDA, TMP; (iii) n-BuLi, 0 °C; (iv) $ZnCl_2$-TMEDA, RT; (v) 2-iodo-5-bromopyridine, $Pd(PPh_3)_4$, reflux for 18 h; (vi) n-BuLi, −100 °C; (vii) $FBMes_2$, RT, 12 h.

contribution (f_1 and f_2) coefficients [14,15].

$$\frac{I}{I_0} = \frac{\tau}{\tau_0} = \frac{f_1}{1 + k_{SV1} * P_{O_2}} + \frac{f_2}{1 + k_{SV2} * P_{O_2}} \quad (1)$$

$$1 = f_1 + f_2 \quad (2)$$

$$k_{SV}^{app} = f_1 k_{SV1} + f_2 k_{SV2} \quad (3)$$

The weighted quenching constant (k_{SV}^{app}) is the parameter which determines the sensitivity of an OSP and is calculated using equation (3).

3. Results and discussion

3.1. Syntheses of compounds 2 and 3, and crystal structure of 2

The synthetic routes of **L1** and **L2** are shown in Scheme 1 and Scheme 2, respectively. Both compounds were prepared via lithiation at −100 °C in dry THF to increase the lithium-halogen exchange selectivity as previously demonstrated by Wang et al. [6]. All other *N*,C-chelates were prepared via literature reported

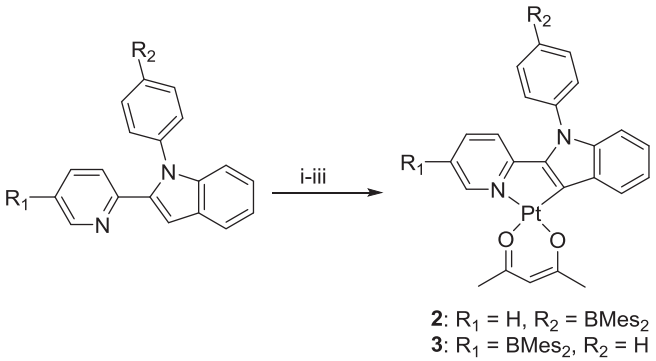

Scheme 3. Synthetic scheme of compounds **2** and **3**. Reaction Conditions: (i) $[PtMe_2(SMe_2)]_2$, THF, RT, 1 h; (ii) *p*-toluenesulfonic acid, THF, RT, 1.5 h (iii) Na(acac), MeOH, RT, 0.5 h.

methods [6–8]. The Pt(II) complexes of **L1** (**2**)and **L2** (**3**) were synthesized by the one-pot procedure developed earlier in our group (Scheme 3) [9]. These complexes were fully characterized by NMR and elemental analyses (see supporting information). The structure of **2** was determined by single-crystal X-ray diffraction analysis and is shown in Fig. 3. The Pt(II) center in **2** adopts a square-planar geometry with similar Pt-C, Pt-N and Pt-O bond lengths relative to those of **7**. However, unlike **7**, which forms a stacked dimer in the crystal lattice with a Pt···Pt separation distance of 3.6921(Å) [6], no strong intermolecular interactions were observed in the crystal lattice of **2**, as indicated by a relatively large Pt···Pt separation distances ranging from 6.739(1) Å to 14.918(1) Å. This is likely caused by the bulky $BMes_2Ph$ unit which is almost orthogonal to the chelate backbone.

3.2. Photophysical properties

The absorption spectra of compounds **1**–**7** in CH_2Cl_2 at 10^{-5} M were recorded and compared (Fig. 4) to evaluate the effects of $BMes_2$-functionalization and different chelate backbones. While the low-energy absorption bands of the complexes with $BMes_2$ group attached to the pyridyl ring of the chelate backbone (**3**, **5** and **7**) show bathochromic shifts of 40–55 nm and are ~1.3–2.6 times more intense compared to their non-borylated counterparts (**1**, **4** and **6**, respectively), which is consistent with what we have observed in other $BMes_2$-functionalized cyclometalated Pt(II) complexes [6], the absorption spectra of **1** and **2** are almost identical, indicating that the $BMes_2$ group has very little contribution to the frontier orbitals of compound **2**, which is in accordance with the

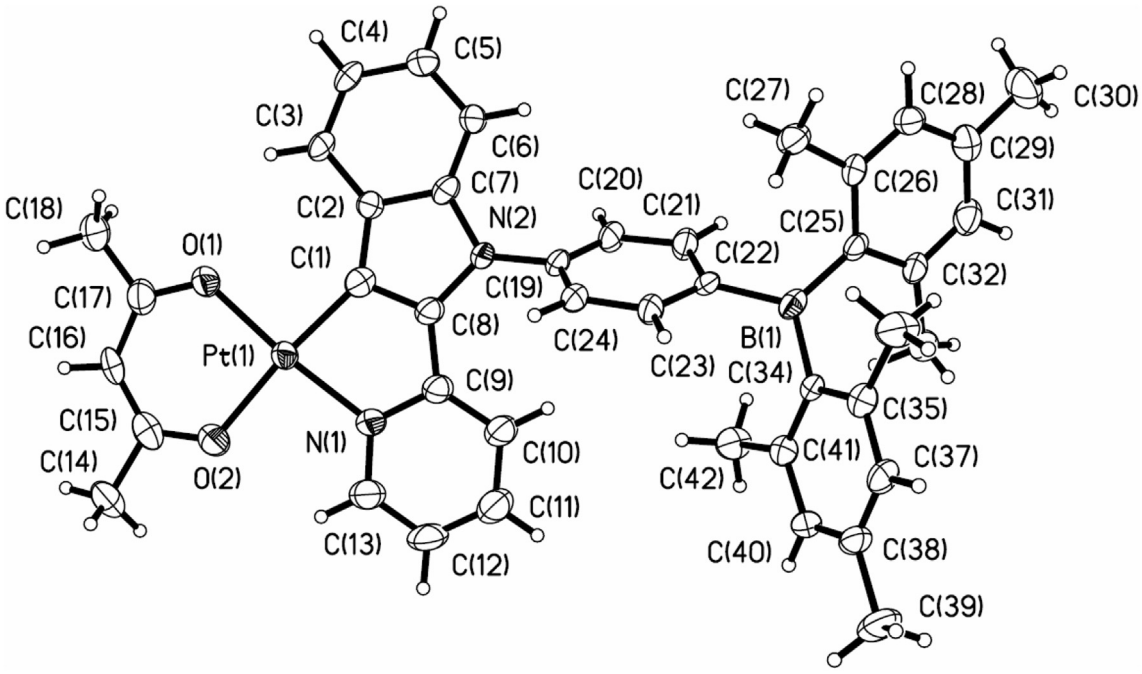

Fig. 3. Crystal structure of **2** with labeling schemes and 35% thermal ellipsoids.

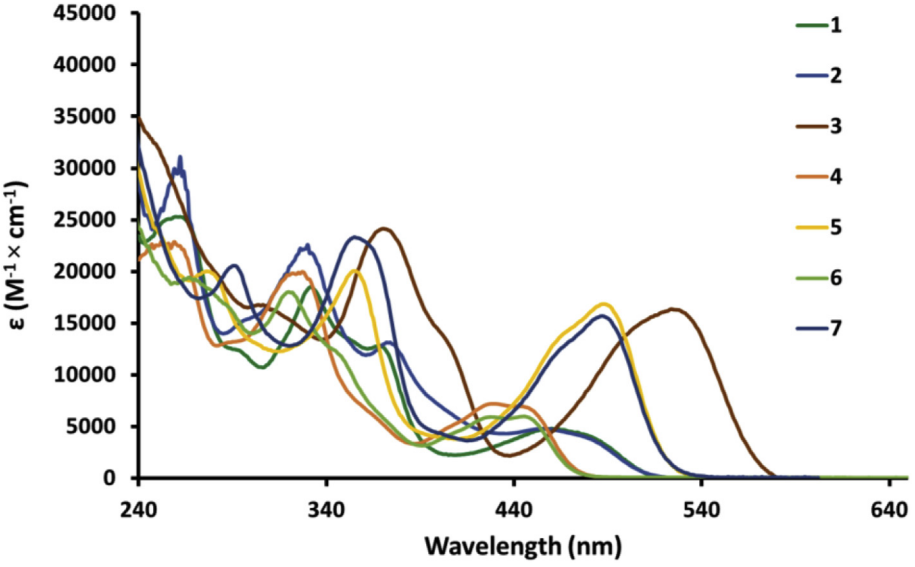

Fig. 4. Absorption spectra of compounds **1**–**7** at 10^{-5} M in CH_2Cl_2.

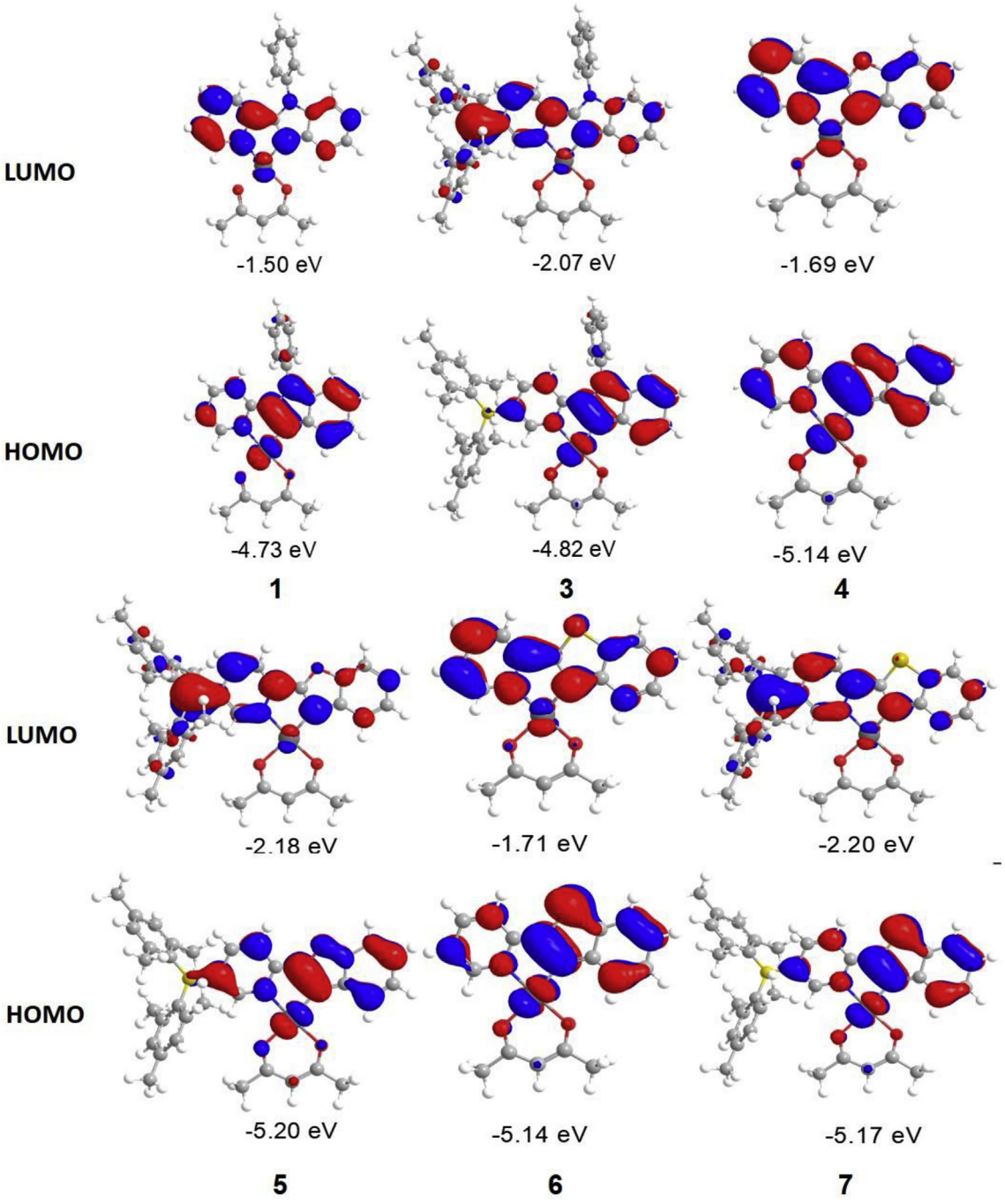

Fig. 5. HOMO and LUMO diagrams of selected compounds (isocontour level = 0.03).

large dihedral angle between the $BMes_2Ph$ moiety and the pyridyl-indole in the crystal structure of **2**. The changes of the chelate backbone from pyridyl-indolyl (**1**) to pyridyl-benzofuryl (**4**) or pyridyl-benzothienyl (**6**) lead to hypsochromic shifts of 25 nm and 27 nm of the low-energy absorption band, respectively. The higher energy bands (320–370 nm) in the absorption spectra of compounds **1**–**7** can be assigned to LC transitions ($\pi \rightarrow \pi^*$ of the chelate ligand) while the lower energy bands (420–530 nm) are typically attributed to mixed metal to ligand charge transfer (MLCT) and LC transitions.

The phenyl-triazole based complexes **8**–**12** all have strong absorption peaks at 340–370 nm that can be assigned to π-π^* transitions of the chelate backbones (Fig. S4A) [7,8]. Additionally, compound **11** has a fairly intense low energy ligand-ligand charge transfer (LLCT) band at ~400 nm which involves mainly the transition from the Ph_2NPh moiety to the pyridyl-1,2,4-triazole ancillary ligand, as indicated by TD-DFT calculation results. The photophysical data are summarized in Table 1.

To gain further understanding of the absorption profiles, TD-DFT calculations were performed for compounds **1**–**7** at the B3LYP level of theory using LANL2DZ for the Pt(II) atom and 6–31 g(d) basis set for all other atoms. TD-DFT calculations established that for

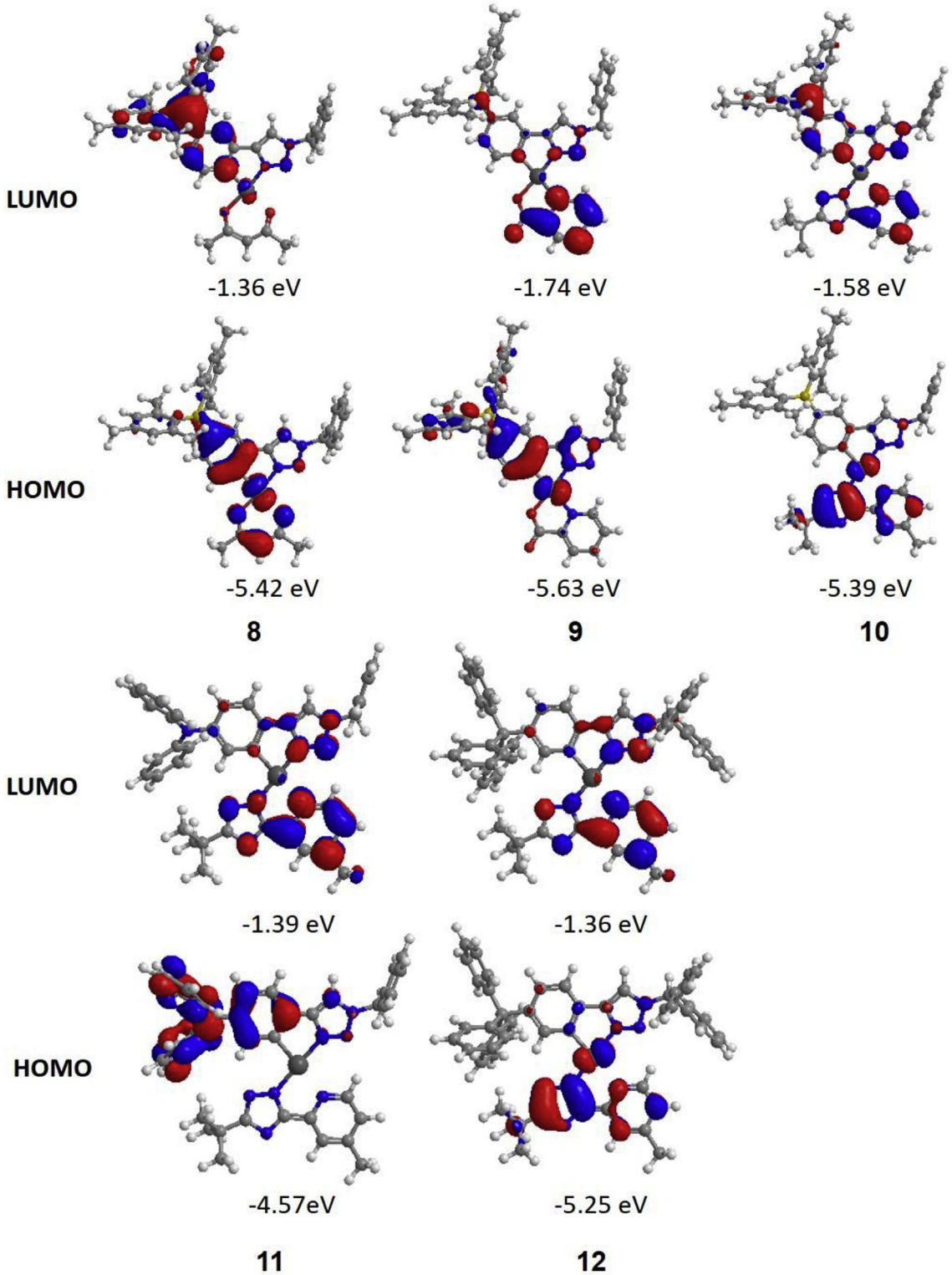

Fig. 6. HOMO and LUMO diagrams of compounds **8**–**12** (isocontour level = 0.03).

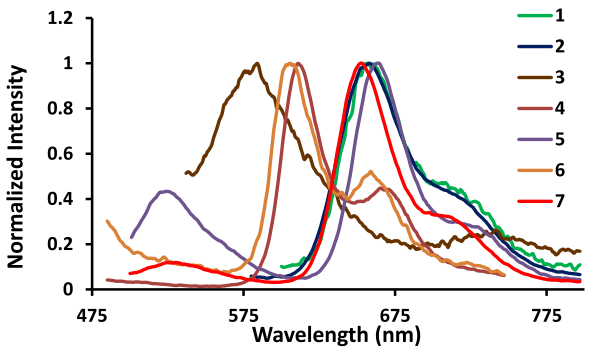

Fig. 7. Normalized emission spectra of compounds **1**–**7** at 10^{-5} M in CH_2Cl_2.

compounds **1** and **3**–**7**, the lowest electronic transitions are dominated by the HOMO→LUMO transition (>89%). For **2**, the $S_0 \rightarrow T_1$ transition mainly consists of HOMO→LUMO+1 transition (69%). The non-borylated compounds **1**, **4** and **6** have their HOMOs situated on the chelate backbone with some contributions from the metal center and their LUMOs is predominantly located on the chelate ligand (Fig. 5), thus the HOMO→LUMO transition can be attributed to an admixture of LC and MLCT transitions. For complexes **3**, **5** and **7**, their HOMOs are similar to those of their non-borylated analogues while their LUMOs are dominated by the electron deficient boron center and the pyridyl ring, which is consistent with previous reports [6]. The predicted spectra (Fig. S3A) revealed that the incorporation of $BMes_2$ group (**3**, **5** and **7**) caused a bathochromic shift of the low energy band, which agrees well with the experimental data.

Theoretical calculations for the phenyl-triazole-based complexes **8**–**12** have been done previously by our group and their frontier orbital diagrams are shown in Fig. 6 [7,8]. It was found that the $S_0 \rightarrow S_1$ transitions of complexes **8**–**12** are dominated by their HOMO→LUMO transitions (>70%), which are also the main contributors to their $S_0 \rightarrow T_1$ transitions (>58%). Based on the frontier orbital diagrams, the lowest electronic transitions of compounds **8**–**12** can be considered admixtures of MLCT transitions and LC/LLCT transitions except for **11**, which consists of predominately LLCT transitions with no contribution from the Pt d orbital.

Upon examining the emission spectra of complexes **1**–**7** at 10^{-5} M in CH_2Cl_2 (Fig. 7), it was observed that the emission profiles of **4** and **6** are nearly identical while that of **1** shows a bathochromic

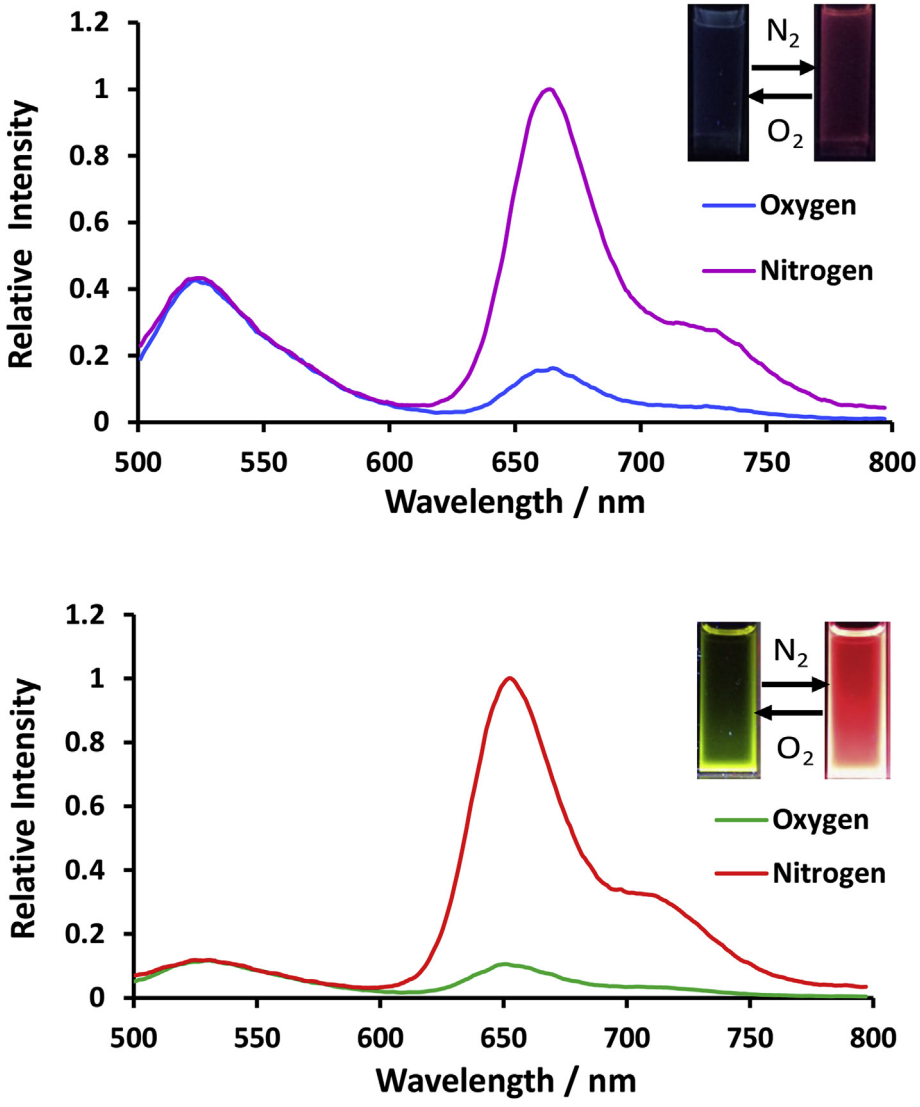

Fig. 8. Emission spectra of **5** (top) and **7** (bottom) under N_2 and O_2 at 10^{-5} M in CH_2Cl_2.

Table 1
Photophysical properties of compounds **1**–**12**.

Complex	Absorption, λ_{max} [nm], ε [10^4 $cm^{-1}M^{-1}$][a]	Emission, 298 K[a]		Emission, 77 K[a]
		λ_{max} [nm]	Φ_P	τ_p (μs)
1	267(2.53), 335(1.79), 372(1.25), 475(0.45)	658	0.04	2.0
2	268(3.13), 328(2.93), 375(1.67), 465(0.48)	657	0.03	4.59
3	226(5.90), 374(2.39), 530(1.61)	581	0.0014	–
4	263(1.57), 330(1.43), 431(0.49), 443(0.70)	611	0.02	6.49
5[ref] [6]	231(3.68), 282(1.93), 357(1.96), 492(1.64)	664	0.06	8.90
6[ref] [16]	226(2.61), 321(1.52), 427(0.53), 445(0.60)	604	0.04	11.3
7[ref] [6]	292(2.05), 357(2.33), 488(1.56)	652	0.12	13.6
8[ref] [7]	326(2.45), 362(2.58)	450	<0.001	27.8
9[ref] [7]	274(1.99), 306(1.68), 358(2.01)	456	<0.001	16.8
10[ref] [7]	321(2.24), 364(3.97)	474	0.10	9.6
11[ref] [8]	314(3.23), 345(3.24)	514	0.21	23.9
12[ref] [8]	276(4.00), 354(1.35)	482/512	0.13	5.3

[a] **1**–**7** were measured in CH_2Cl_2 at 1×10^{-5} M. **8**–**10** were measured in 2-methyltetrahydrofuran at 2×10^{-5} M. **11** and **12** were measured in CH_2Cl_2 at 2×10^{-5} M.

Table 2
Properties of the O_2-sensing film of **1**–**12** (except **3**) with EC as the supporting matrix (fitting of the experimental data to equation (1)).

Compound	f_1[a]	f_2[a]	k_{SV1} ($torr^{-1}$)[b]	k_{SV2} ($torr^{-1}$)[b]	r^2	k_{SV}^{app}($torr^{-1}$)[c]	P_{O_2} (torr)[d]
1	0.860	0.140	0.0184	0	0.986	0.0158	63
2	0.895	0.105	0.0188	0	0.979	0.0168	60
4	0.898	0.103	0.0203	0	0.995	0.0182	55
5	0.931	0.0687	0.0307	0	0.986	0.0285	35
6	0.939	0.0614	0.0234	0	0.984	0.0221	45
7	0.955	0.0447	0.0368	0	0.981	0.0351	28
8	0.764	0.236	0.0255	0	0.997	0.0195	51
9	0.824	0.176	0.00596	0	0.988	0.00491	204
10	0.901	0.0986	0.0240	0	0.994	0.0217	46
11	0.996	0.0038	0.0669	0	0.993	0.0667	15
12	0.917	0.0827	0.0120	0	0.995	0.0110	91

[a] Ratio of the two portions of the Pt(II) complex.
[b] Quenching constant of the two portions.
[c] Weighted quenching constant.
[d] The oxygen partial pressure at which the initial emission intensity of the film is quenched by 50% and calculated as $1/K_{sv}^{app}$, in torr.

shift of ~47 nm. The addition of $BMes_2$ group to the pyridyl ring of **4** ($\lambda_{max} = 611$ nm, $\Phi = 0.02$) and **6** ($\lambda_{max} = 604$ nm, $\Phi = 0.04$) leads to emission energy redshifts of 53 nm and 48 nm, respectively, as well as tripled phosphorescent quantum yields. It is worth noting that compounds **5** and **7** show dual emission, with the high energy band at ~525 nm being insensitive towards oxygen, which can be assigned to fluorescence, while the low energy peaks at 664 nm (**5**) and 652 nm (**7**) are readily quenched in the presence of oxygen, as depicted in Fig. 8. Interestingly, attaching the $BMes_2$ group to the phenyl ring and pyridyl ring of **1** ($\lambda_{max} = 658$ nm, $\Phi = 0.04$) results in 1 nm and 77 nm blueshifts in emission energy, respectively, accompanied with reduced quantum yields ($\Phi = 0.03$ and 0.0014, respectively). The phosphorescence decay lifetimes of the $BMes_2$-functionalized compounds **2** (4.59 μs), **5** (8.90 μs) and **7** (13.6 μs) are longer than their non-borylated analogues (2.0 μs, 6.49 μs and 11.3 μs, respectively), which makes them better candidates as luminescent OSPs.

The emission spectra of compounds **8**–**12** are shown in Fig. S4B [7,8]. The $BMes_2$-functionnalized phenyl-triazole complexes **8**–**10** display blue phosphorescence ($\lambda_{max} = 450$–474 nm) in 2-Methyl-THF with low quantum yields (≤0.1). As previously reported, these compounds have a greater tendency to undergo collisional quenching with the solvent molecules. The higher emission quantum yield of **10** relative to those of **8** and **9** could be attributed to the higher ligand field strength of pytrz-*t*Bu compared to those of acac and pic, which makes the non-emissive metal DMSO-d_6 state thermally inaccessible. Compounds **11** and **12** display green ($\lambda_{max} = 514$ nm) and greenish-blue ($\lambda_{max} = 486/512$ nm) phosphorescence with moderate phosphorescence quantum yields of 21% and 13%, respectively. The enhancement of Φ_P of **11** and **12** compared to that of **10** could be attributed to the diphenyl amine/trityl group at the position *meta* to the Pt atom in **11** and **12** which are more effective in shielding the Pt center and preventing intermolecular interactions than the $BMes_2$ groups at the position *para* to the Pt atom in **10**. The phosphorescence lifetime of compounds **8**–**10** decrease in the following order: **8** (27.6 μs) > **9** (16.8 μs) > **10** (9.6 μs), which can be ascribed to the ligand field strength of the ancillary ligands, which increases following the order of acac (**8**) < pic (**9**) < pytrz-*t*Bu (**10**). The longer phosphorescence lifetime of **11** relative to that of **12** can be explained by less involvement of the Pt d orbital in the S_0-T_1 transitions, as discussed earlier.

3.3. Oxygen sensing

The oxygen sensing abilities of compounds **1**–**12** in polymer matrices were investigated by doping the Pt(II) complexes in ethyl cellulose (EC) films at 5 wt% (**1**–**7**) and 1 wt% (**8**–**12**), respectively, owing to that the emission of compounds **8**–**12** on solid support is much brighter than that of **1**–**7**. The emission of **3** in 5 wt% EC films is too weak to obtain a reliable EL spectrum and will not be discussed further. An operational stability test was first conducted by monitoring the emission intensities of the oxygen sensing films during 8 cycles of switching between pure N_2 and pure O_2 in a duration of 4000s. The dynamic responses of the oxygen sensing films towards oxygen were investigated by varying the O_2 partial pressure using a flowmeter, and the data were fitted using equation (1). The oxygen sensing data of **1**–**12** (except **3**) in EC films are shown in Table 2.

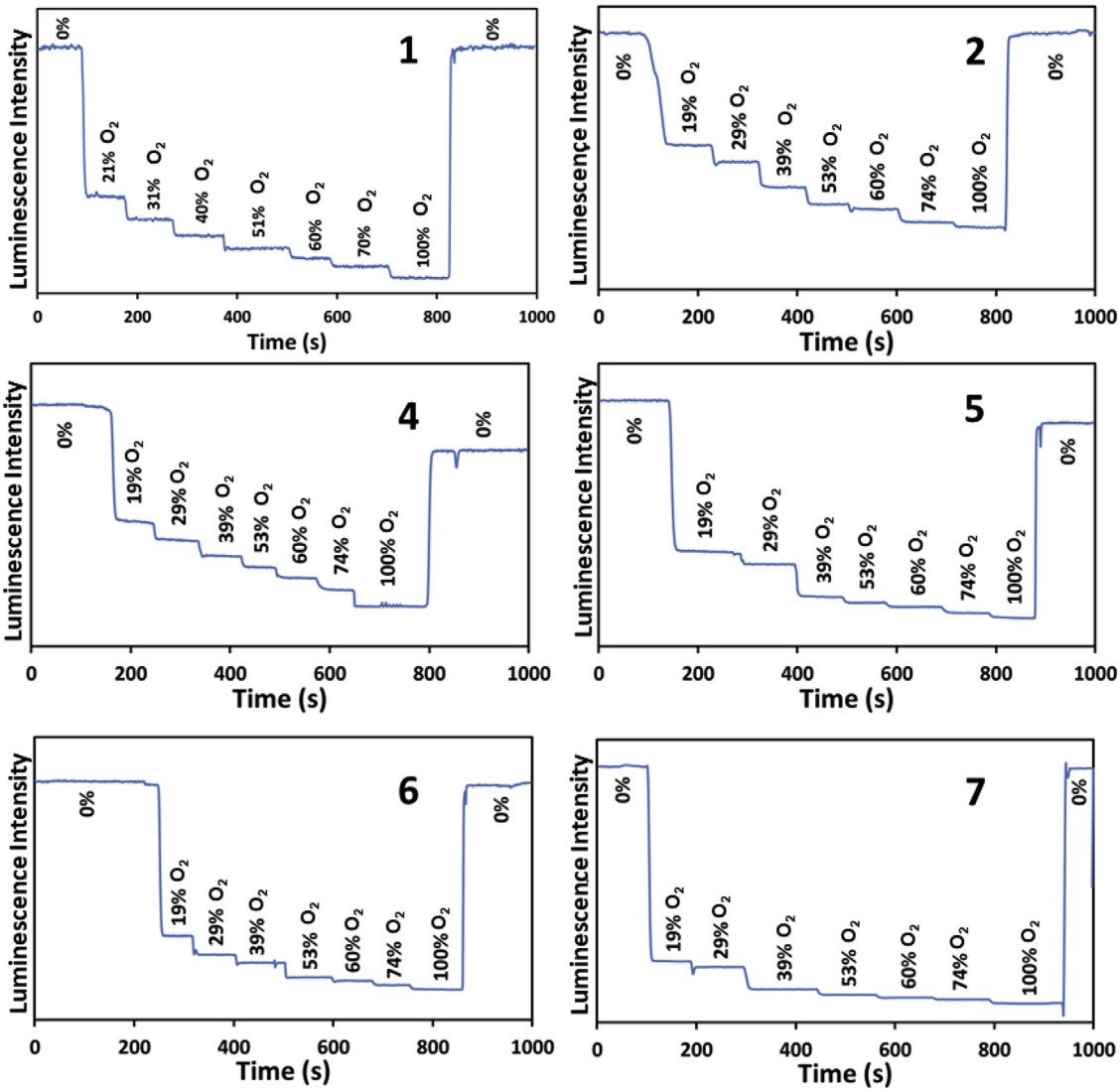

Fig. 9. Dynamic emissive intensity response of oxygen sensing films of oxygen sensing films of **1**, **2** and **4**–**7** under varying concentrations of O_2, at 25 °C.

*Compounds **1**–**7***. As shown in Fig. S5A, the EC films of the pyridyl-indole based compounds (**1** and **2**) and the pyridyl-benzothiophene based compounds (**6** and **7**) show good operational stabilities as their PL intensity under pure N_2 shows no decrease after 8 cycles of switching between N_2 and O_2 and the quenching and recovering cycles are fully reversible. On the other hand, the operational stabilities of the EC films of the pyridyl-benzofuran based compounds (**4** and **5**) are not good, as indicated by the decrease of I_0 during the stability test (Fig. S4A), suggesting that the pyridyl-benzofuran chelated Pt(II) complexes may not be suitable as OSPs. The responses of emission intensity of the oxygen sensing films towards step-wise increased O_2 concentrations are shown in Fig. 9 and the data are fitted using equation (1) (Fig. 10). The K_{SV}^{app} values derived from the Stern-Volmer curves reveal that the change of the chelate ligand from pyridyl-indole to phenyl-benzofuran to pyridyl-benzothiophene and the attachment of the $BMes_2$ group lead to increased oxygen sensitivity, indicating that borylation is a viable strategy to increase the sensitivities of OSPs.

*Compounds **8**–**12***. Compounds **8**–**10** were doped in EC at 1% wt, which displayed O_2 quenchable luminescence as depicted in Fig. 11. The stability tests (Fig. S5B) revealed that all three species are photobleached after several cycles of purging with N_2 and O_2 gases and the photobleaching of **8** is the most pronounced. This could be attributed to the extra stability provided by the intramolecular hydrogen bonds in compounds **9** ($N_{trz}\cdots H_{Py}$) and **10** ($N_{1,2,3\text{-}trz}\cdots H_{Py}$ and $N_{1,2,4\text{-}trz}\cdots H_{Ph}$), which is absent in **8** [7,8]. Upon examining their relative oxygen sensitivities (Fig. 12), the k_{SV}^{app} value for **10** (0.0217 $Torr^{-1}$) is higher than those of **8** (0.0195 $Torr^{-1}$) and **9** (0.00491 $Torr^{-1}$), despite its shorter phosphorescence decay lifetime, which is inconsistent with literature findings[1] and requires further studies.

We next turned our attention to compounds **11** and **12** which are modified versions of compound **10** in which the dimesitylboron unit is replaced with a diphenylamino unit (**11**) and a triphenyl methyl unit (**12**), respectively. The emission of the EC films of both **11** and **12** was quenched with the step-wise addition of O_2 (Fig. 11). Purging with 8 cycles of N_2 and O_2 gases revealed that the oxygen sensing film of **12** is photostable while that of **11** is slightly bleached (Fig. S4B). As shown in Fig. 12, compound **12** has an average k_{SV}^{app} of 0.011 $Torr^{-1}$ while that of **11** is very impressive (0.0667 $Torr^{-1}$), which is the highest among compounds **1**–**12** and is much higher

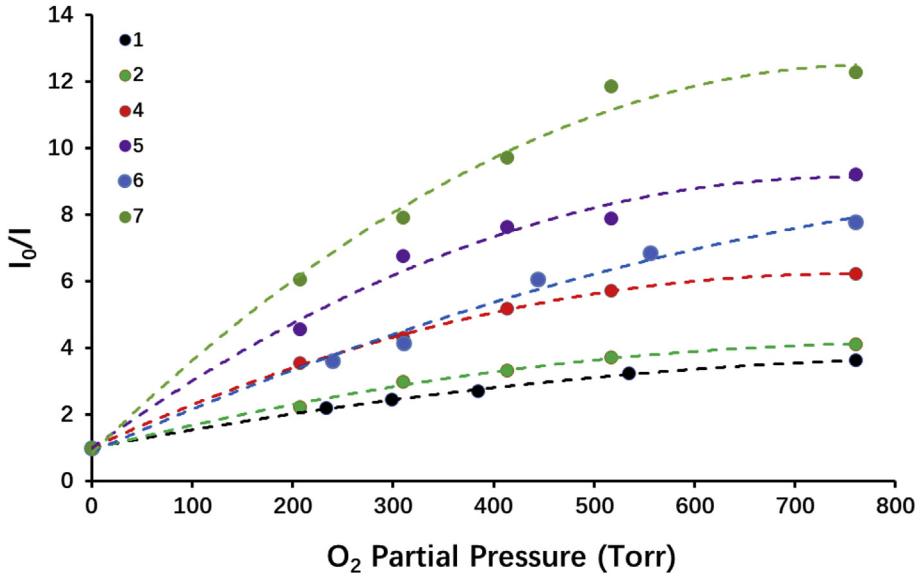

Fig. 10. Stern-Volmer plots for oxygen sensing films of **1**, **2** and **4**–**7** (intensity ratios I_0/I versus O_2 partial pressure).

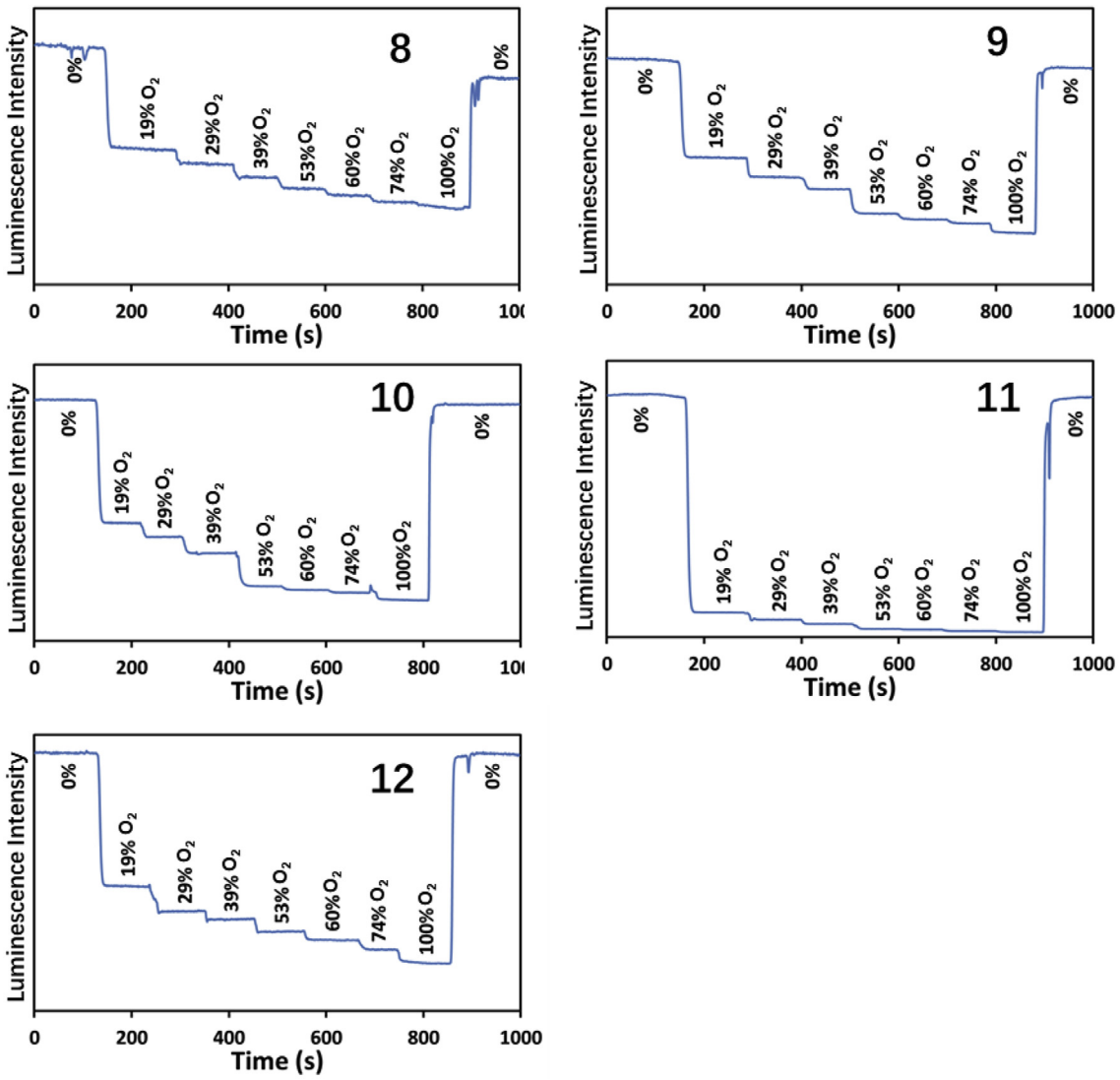

Fig. 11. Dynamic emission intensity response of oxygen sensing films of **8**–**12** under varying concentrations/partial pressures of O_2 in N_2, at 25 °C.

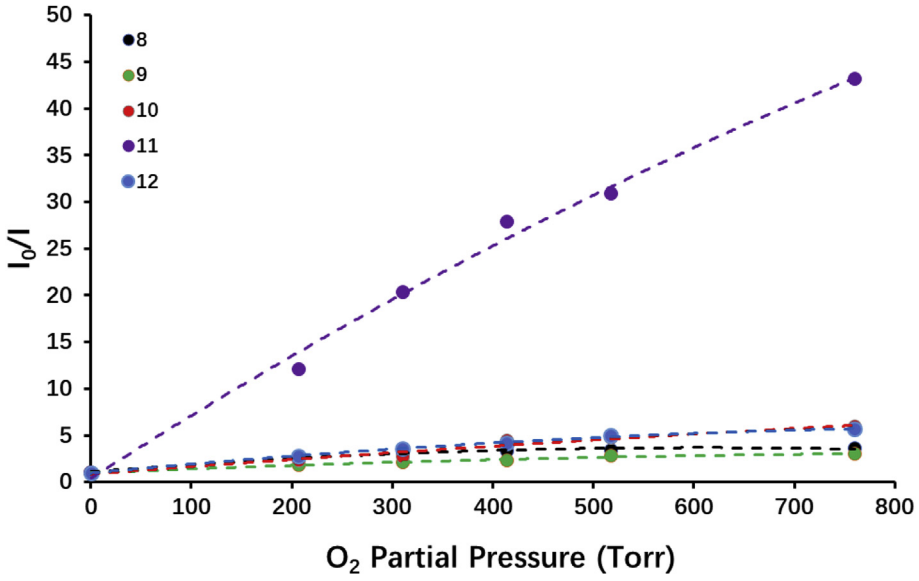

Fig. 12. Stern-Volmer plots for oxygen sensing films of **8**–**12** (intensity ratios I_0/I versus O_2 partial pressure).

than recently reported fluorine-containing Ir(III) and Pt(II) complexes ($K_{sv}^{app} < 0.021\,Torr^{-1}$) [14,15]. This can be attributed to compound **11**'s long phosphorescence decay lifetime that enables increased interaction time with O_2, leading to the drastically enhanced luminescence quenching. This finding demonstrates that luminescent Pt(II) complexes with minimal MLCT transitions in the $S_0 \rightarrow T_1$ transition may be good candidates for luminescent OSPs with a high sensitivity.

4. Conclusions

The synthesis of two new Pt(II) complexes functionalized by a dimesitylboron unit was achieved. By comparing the oxygen sensitivity of a group of bidentate Pt(II) complexes with a range of *N*,C-chelates and ancillary ligands in EC films, several interesting observations were made which could aid the future design of luminescent OSPs with a high oxygen sensitivity and operational stability. First, pyridyl-benzofuran based bidentate Pt(II) compounds are less photostable compared to their pyridyl-indole and pyridyl-benzothiophene chelated counterparts. Second, borylation seems a facile strategy for simultaneously increasing the quantum yields and the oxygen sensitivity of the Pt(II) based OSPs. Third, phosphorescent Pt(II) complexes with the T_1 state consisting of predominately intra-ligand CT or LLCT transitions may be highly effective in achieving highly sensitive luminescent OSPs, owing to their high quantum yields and long phosphorescent decay lifetimes.

Acknowledgment

We thank the natural sciences and engineering research council of Canada for financial supports.

Appendix A. Supplementary data

Supplementary data to this article can be found online at https://doi.org/10.1016/j.jorganchem.2018.11.017.

References

[1] X.D. Wang, O.S. Wolfbeis, Chem. Soc. Rev. 43 (2014) 3666–3761.
[2] (a) L. Huynh, Z. Wang, J. Yang, V. Stoeva, A. Lough, I. Manners, M.A. Winnik, Chem. Mater. 17 (2005) 4765–4773;
(b) C.S.K. Mak, D. Pentlehner, M. Stich, O.S. Wolfbeis, W.K. Chan, H. Yersin, Chem. Mater. 21 (2009) 2173–2175;
(c) A. Ruggi, M. Berenguel Alonso, D.N. Reinhoudt, A.H. Velders, Chem. Commun. (J. Chem. Soc. Sect. D) 46 (2010) 6726–6728.
[3] (a) D. Garcia-Fresnadillo, G. Orellana, M.D. Marazuela, M.C. Moreno-Bondi, Langmuir 15 (1999) 6451–6459;
(b) A. Mills, M. Thomas, Analyst 122 (1997) 63–68;
(c) Y. Amao, I. Okura, Sens. Actuators, B 88 (2003) 162–167;
(d) I. Gryczynski, J. Malicka, E. Holder, N. DiCesare, J.R. Lakowicz, Chem. Phys. Lett. 372 (2003) 409–414.
[4] (a) E.M. Kober, J.L. Marshall, W.J. Dressick, B.P. Sullivan, J.V. Caspar, T.J. Meyer, Inorg. Chem. 24 (1985) 2755–2763;
(b) W. Xu, K.A. Kneas, J.N. Demas, B.A. DeGraff, Anal. Chem. 68 (1996) 2605–2609.
[5] (a) Y. Amao, I. Okura, T. Miyashita, Bull. Chem. Soc. Jpn. 73 (2000) 2663–2668;
(b) S. Borisov, I. Klimant, Anal. Bioanal. Chem. 404 (2012) 2797–2806;
(c) Y. Wang, B. Li, L. Zhang, Q. Zuo, P. Li, J. Zhang, Z. Su, ChemPhysChem 12 (2011) 349–355.
[6] Z.M. Hudson, C. Sun, M.G. Helander, H. Amarne, Z.-H. Lu, S. Wang, Adv. Funct. Mater. 20 (2010) 3426–3439.
[7] X. Wang, Y.-L. Chang, J.-S. Lu, T. Zhang, Z.-H. Lu, S. Wang, Adv. Funct. Mater. 24 (2014) 1911–1927.
[8] X. Wang, S.-L. Gong, D. Song, Z.-H. Lu, S. Wang, Adv. Funct. Mater. 24 (2014) 7257–7271.
[9] Z.M. Hudson, B.A. Blight, S. Wang, Org. Lett. 14 (2012) 1700–1703.
[10] M.J. Frisch, G.W. Trucks, H.B. Schlegel, G.E. Scuseria, M.A. Robb, J.R. Cheeseman, G. Scalmani, V. Barone, B. Mennucci, G.A. Petersson, H. Nakatsuji, M. Caricato, X. Li, H.P. Hratchian, A.F. Izmaylov, J. Bloino, G. Zheng, J.L. Sonnenberg, M. Hada, M. Ehara, K. Toyota, R. Fukuda, J. Hasegawa, M. Ishida, T. Nakajima, Y. Honda, O. Kitao, H. Nakai, T. Vreven, J.A. Montgomery Jr., J.E. Peralta, F. Ogliaro, M. Bearpark, J.J. Heyd, E. Brothers, K.N. Kudin, V.N. Staroverov, R. Kobayashi, J. Normand, K. Raghavachari, A. Rendell, J.C. Burant, S. Iyengar, J. Tomasi, M. Cossi, N. Rega, J.M. Millam, M. Klene, J.E. Knox, J.B. Cross, V. Bakken, C. Adamo, J. Jaramillo, R. Gomperts, R.E. Stratmann, O. Yazyev, A.J. Austin, R. Cammi, C. Pomelli, J.W. Ochterski, R.L. Martin, K. Morokuma, V.G. Zakrzewski, G.A. Voth, P. Salvador, J.J. Dannenberg, S. Dapprich, A.D. Daniels, O. Farkas, J.B. Foresman, J.V. Ortiz, J. Cioslowski, D.J. Fox, Gaussian 09, Revision E.01, Gaussian, Inc., Wallingford CT, 2009.
[11] S.K. Mellerup, Y.-L. Rao, H. Amarne, S. Wang, Org. Lett. 18 (2016) 4436–4439.
[12] K. Grudzień, B. Trzaskowski, M. Smoleń, R. Gajda, K. Woźniak, K. Grela, Dalton Trans. 46 (2017) 11790–11799.
[13] J.N. Demas, B.A. DeGraff, W. Xu, Anal. Chem. 67 (1995) 1377–1380.
[14] Y. Xing, C. Liu, J. Xiu, J. Li Inorg. Chem. 54 (2015) 7783–7790.
[15] C. Liu, X. Lv, Y. Xing, J. Qiu, J. Mater. Chem. C 3 (2015) 8010–8017.
[16] J. Brooks, Y. Babayan, S. Lamansky, P.I. Djurovich, I. Tsyba, R. Bau, M.E. Thompson Inorg, Chem. 41 (2002) 3055–3066.